Measurements of the population partitions and state-selected flight-time distributions of keV ion-beam-sputtered metastable atoms

E. Vandeweert, P. Lievens, V. Philipsen, J. Bastiaansen, and R. E. Silverans
Laboratorium voor Vaste-Stoffysica en Magnetisme, Katholieke Universiteit Leuven, Celestijnenlaan 200 D, B-3001 Leuven, Belgium
(Received 28 December 2000; revised manuscript received 2 April 2001; published 29 October 2001)

A sensitive and generally applicable experimental procedure to determine the relative population on different quantum states of free metastable atoms is presented. The atoms are both element and state-selectively ionized using highly efficient double-resonant two-color two-step laser ionization. Population partitions can be quantitatively measured by extending the procedure to include all metastable states. In combination with a pulsed atom source, state-selective flight-time distributions can be measured. Such experiments allow one to evaluate the kinetic energy of the released atoms. The methodology is demonstrated and fully commented with the measurement of the population partition of gas-phase atoms released from a hot Ni filament. A systematic study of the emission of neutral atoms during 15 keV Ar^+ sputtering of clean polycrystalline Co and Ni foils is reported, illustrating that sets of population partitions and flight-time distributions can be obtained with the presented experimental procedure. The combined interpretation of the experimental evidence allows one to qualitatively model the emission of excited atoms during sputtering of metals as the result of a multichannel electron transfer process. In this model, a sputtered particle escapes from the surface as a positive ion and becomes neutralized into an atomic state by resonant transfer of an electron from the valence band of the metal. The velocity-dependent population of a particular state is governed by the correspondence of the electronic configuration of the atomic state with the bulk electronic configuration.

DOI: 10.1103/PhysRevB.64.195417 PACS number(s): 79.20.Rf, 32.80.Fb, 32.80.Rm

I. INTRODUCTION

Many vapor deposition techniques as well as sophisticated analytical characterization methods rely on the emission of particles during and after a violent interaction between an incident projectile and a solid substrate. Depending on the type and intensity of the primary particle beam and the nature of the target, the release of material is the result of a complex interplay of thermal, ballistic and hydrodynamical mechanisms and the overall processes are classified using an abundance of nomenclature.[1–5] For sake of clearness we retain here only laser or ion-beam sputtering to denote photons resp. energetic ions impinging on a metallic substrate. Although highly desirable, not in the least from a fundamental physical point of view, a thorough understanding of many aspects of these sputter mechanisms is often still lacking.

The sputtered particles are mainly atoms, molecules or small clusters distributed among different charged and electronic states, often with neutral atoms being the dominant contribution. These atoms are further characterized by their internal and kinetic energies. A well-known example is the energy partition of an ideal gas in thermal equilibrium at a constant temperature. The atoms are then distributed over the available electronic energy levels with kinetic energies according to the underlying Maxwell-Boltzmann statistics. Such a thermodynamic equilibrium cannot *a priori* be assumed to exist during all phases of a laser or ion sputtering event. But also for such processes theoretical descriptions predict specific properties of the emitted atoms.[1–5] For example, in many experiments the kinetic energy distributions of atoms sputtered during ion-induced collision cascades were found to correspond to a good approximation to the so-called Thompson distribution, which is discussed in more detail below.[6,7] The main kinematic aspects of an ion-induced sputter event such as the overall yield or the energy- or angular-resolved distributions are reasonably well described by the transfer of impact energy and momentum during a collision cascade initiated by an incident energetic particle. However, processes involved in the determination of the final electronic state of a sputtered atom are much less understood. In this respect, experimentally observed population partitions and state-selective kinetic energy distributions are key observables to gain more insight in the importance of electronic processes involved in such processes. Over the years, this subject has drawn the attention of numerous researchers. For a detailed overview of the early measurements using fluorescence techniques, the reader is referred to Ref. 8. The results allowed us to draw a crude correlation between the formation of excited atoms during the sputter event and their fundamental properties. The application of resonant laser-ionization spectroscopy (RIS) recently allowed us, amongst other workers, to gather new experimental evidence that helps to refine our understanding on the electronic processes involved during ion-beam sputtering.[9–27] These experiments are based on the state-selective ionization of free atoms by RIS. They focus on the charge-sensitive detection of abundantly sputtered metastable atoms (having lifetimes of the order of seconds) that preserve their excitation state even at large distances from the surface.

Resonance laser-ionization spectroscopy is an experimental technique that is highly favored because of its unmatched sensitivity and selectivity.[28] A typical RIS experiment is a two-step experiment. In the first step, the metastable atoms are resonantly excited into a high lying state by resonant absorption of a photon. But before the highly excited atom has time to decay from this intermediate state, the absorption of at least one other photon brings the atom above its ioniza-

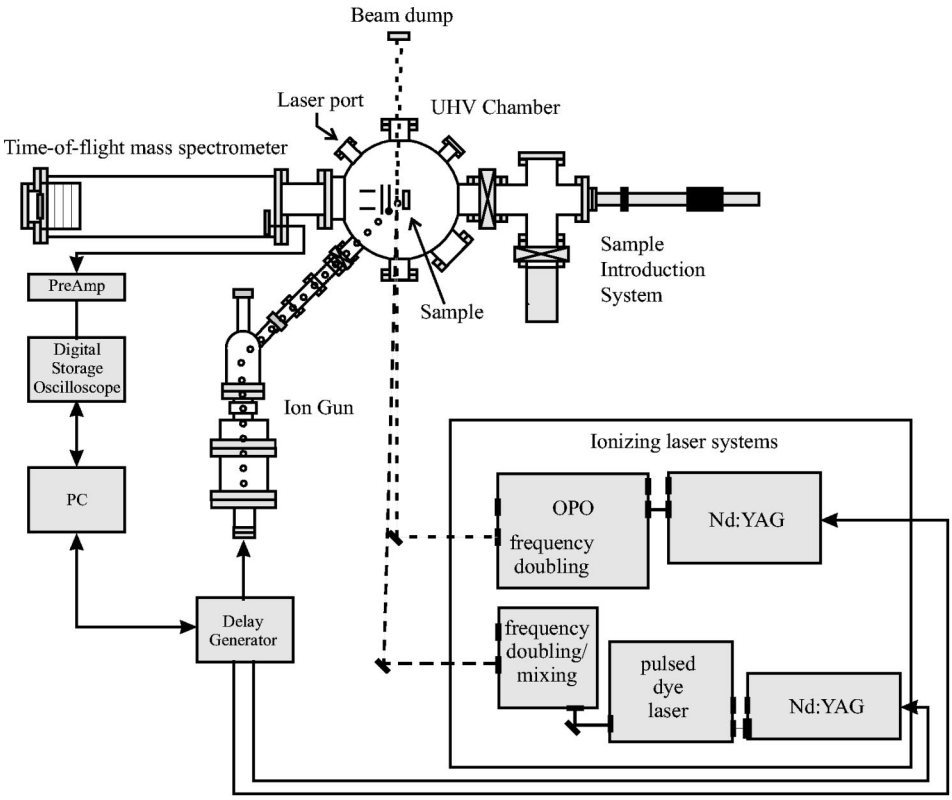

FIG. 1. Schematic presentation of the resonance ionization mass spectrometry setup.

tion limit. Since each element has a unique set of atomic energy levels, the excitation step of the ionization scheme ensures not only element but also quantum-state selectivity of the overall RIS process. Most atomic states of almost all elements are known and their properties are extensively tabulated. Hundreds of ionization schemes are documented in literature. Efforts have been made to compile this information in a database. Part of these compilations have been published by Salomon and serve as an excellent reference to suitable ionization schemes but also to previously published RIS work for many elements.[29–32]

If only one tunable laser system is used and a photon from the same laser source is used during the ionization step, the ionization scheme is called a one-color two-step scheme. In a two-color two-step ionization scheme, the excitation and the ionization step are driven each by their own tunable laser system. Since continuum structures are known to induce large variations in the values for the cross sections for photoionization, two-color two-step ionization schemes can be designed to take advantage of this by including an autoionizing state in the ionization step.[28] Although a second laser system has to be implemented, such double-resonant ionization schemes are highly favored since the highest achievable ionization efficiency (by ionizing every atom of interest present in the ionization volume during the laser pulse) can already be obtained at relatively low laser powers.

In this paper we provide a full discussion on the experimental setup and procedures that were developed and applied to assess population partitions of gas phase atoms. The method is evaluated for a thermal distribution of atoms released from a hot Ni filament. Details on our earlier studies of the emission of neutral atoms upon ion bombardment of clean polycrystalline Co[23] and Ni[21] foils are given. We end with an interpretation of the obtained data sets to elucidate the dominant electronic process responsible for the emission of atoms in metastable states.

II. EXPERIMENTAL SETUP

The experiments were performed with the resonance ionization mass spectrometer (RIMS) shown schematically in Fig. 1. Different atomization methods are available to produce atoms in an UHV environment [base pressure of about 1×10^{-10} hPa maintained by a combination of a differential ion pump and a titanium sublimation pump with a liquid nitrogen cooled cryoshield (Perkin Elmer TNB-X system)]. A fast-entry load lock allows one to transfer samples to and from the sample stub inside the chamber using a transfer probe. This allows quick changes of samples without disrupting the vacuum in the main chamber. The sample stub is attached to a $XYZ\theta$ manipulator that allows translation in three perpendicular directions with an accuracy of 0.04 mm and rotation in the horizontal XY plane.

A differentially pumped ion gun (Atomika A-DIDA W-610) was used to produce Ar^+ ions with kinetic energies variable between 3 and 15 keV. A homebuild electro-optical assembly allows one to separate neutralized gas ions from the ion beam and to operate the ion gun in a pulsed or in a continuous mode at ion-beam currents of $\sim$1.5 μA on a spot with a typical diameter of 3 mm. Pulses of primary ions with a duration down to 200 ns are generated by applying short high voltage pulses on a pair of deflection plates generated by a push-pull switch (Behlke GHTS 60A). The projectiles finally hit the centrally located target at 45° incidence

angle. Experiments on laser-sputtered and thermally produced atoms can be performed in this RIMS setup under exactly the same geometrical and environmental conditions as the experiments on atoms produced by ion-beam sputtering. Therefore a fused silica window allows to direct a laser beam at 45° onto the target. The sample holder can be replaced by a small oven. In this oven, metallic filaments are heated resistively to temperatures up to 2300 K.

The sputtered or thermally evaporated neutrals are state-selectively laser ionized and electrostatically extracted and focused into a time-of-flight mass spectrometer that can be operated either in linear or reflectron mode (R.M. Jordan Cie. AREF-850). When used in combination with a pulsed atom source (e.g., by using short primary ion pulses) the mass spectrometer can be gated to reject secondary ions formed at the surface during the sputtering process. Only atoms sputtered in a narrow polar angle of $\sim 10°$ around the surface normal are allowed to enter the reflectron mass spectrometer. The photoions are detected mass selectively with a mass resolution of about 1000 at 58 amu by a dual microchannel plate detector. The ion signals are amplified (EG&G Ortec 535 Quad Fast Amplifier) before being sent to a digital storage oscilloscope (Tektronix TDS 420) which is connected to an IBM compatible PC via an IEEE-488 interface bus. The setup is triggered by digital delay generators (Stanford Research Systems DG535) at a repetition rate of 10 Hz.

The wide spectral range needed for the laser ionization experiments is supplied by two independent tunable laser systems. An optical parametric oscillator [Spectra-Physics (SP) MOPO 730] pumped by the third harmonic output of a Nd:YAG (SP GCR 230-10) and equipped with a frequency doubling option (SP FDO) can deliver continuously tunable radiation between 220 up to 1600 nm, except in a gap between 690 to 730 nm (345 to 365 nm after frequency doubling) around the degeneracy point. The second laser system is a tunable dye laser (SP PDL 3) with frequency doubling and mixing options (SP WEX 1) and pumped by the second harmonic output of another Nd:YAG laser (SP GCR 12). Both systems provide pulsed linearly polarized ($>95\%$) laser light with a duration of about 6 ns and linewidths ranging from 6 GHz (visible) to 15 GHz (UV) and pulse energies between 3 mJ in the UV up to 50 mJ in the visible. The spatial photon distributions of the loosely focused laser beams are monitored by a CCD camera (Cohu 4800) and are found to have a near Gaussian profile with a diameter of less than 1 mm. The plume of atomized particles is intersected parallel to the sample holder by the two overlapping laser beams and the distance between the target and the laser ionization volume can be varied between 1 and 6 mm. This distance is determined with an accuracy of about 0.1 mm by moving the target holder through the ionization laser beam until half of the laser beam cross section was blocked. This procedure also allows us to critically position the sample surface parallel to the ionizing laser beam and the extraction hole of the mass spectrometer.

III. EXPERIMENTAL PROCEDURES

A. Sample cleaning

Before the actual measurement, the metal surface is *in situ* sputter cleaned by prolonged rastering of the ion beam across the sample to ensure the removal of O, C, and H containing species which are known to form surface layers with a thickness of a few nm.[35] Therefore a continuous beam of Ar^+ ions of 20 $\mu A/cm^2$ is used to remove a few hundred atom layers prior to the actual experiment. Subsequently, the experiment is performed with the ion beam positioned in the middle of the created crater. Because the ion yield depends exponentially on the condition of the surface, secondary ion mass spectrometry is known to be a highly sensitive method to determine the cleanliness of the sample.[36] After rastering, a dramatic decrease in the positive secondary ion yield is observed and, within the instrumental detection limit, ion signals stemming from contaminants disappear. Furthermore, this cleaning procedure is evaluated by a series of independent low-energy ion scattering (LEIS) experiments. In these experiments 2 keV He^+ ions are scattered at polycrystalline foils identical to the ones used in the sputtering experiments. By measuring the scattered ion signal as function of the kinematic factor K, being the ratio of the kinetic energy of the He^+ ion after (E_1) and before ($E_0 = 2$ keV) scattering, the composition of the surface layer of the sample can be determined. Since absolute values for the cross sections for He^+ scattering at low energies are in most cases not reliable and large differences in the (matrix dependent) neutralization efficiency during scattering of the projectiles at atoms of different elements occur, quantification is only possible using standards. In Fig. 2, LEIS spectra obtained from polycrystalline Co and Ni foils (Goodfellow, 99.9% pure) are compared before and after sputter cleaning. The spectra before cleaning are typically observed for oxidized metal surfaces containing traces of Na, K, and hydrocarbons. The foils were then subjected to a prolonged sputtering with 2 keV He^+. Taking into account the differences in sputter yield on clean surfaces due to the difference in kinetic energy and mass of the He and Ar projectiles in the two experiments,[37] care was taken that about the same number of atoms were removed upon completion of the sputter cleaning. The right panels in Fig. 2 show an essentially clean surface for both metals with only submonolayer traces of oxygen and, within the limit of the sensitivity of the method in the experimental setup (being of the order of 10^{-4} of a monolayer), complete absence of any carbon signal.

B. Population partitions

The experimental procedure to determine the relative population of atoms on different metastable states, is based on two-color two-step resonance laser ionization and exemplified schematically for two states in Fig. 3(a). During the first step the atoms are sequentially excited from the envisaged metastable states into a selected intermediate state. During an independent ionization step, the atoms are ionized and counted. If the same intermediate state, and thus the same ionization step, is used for photoionization sequences starting from different metastable states and the excitation steps are saturated, then the measured relative photoion signals will be directly proportional to the initial relative populations of the states. Saturation of the excitation steps can easily be obtained, even at moderate laser pulse energies, by selecting

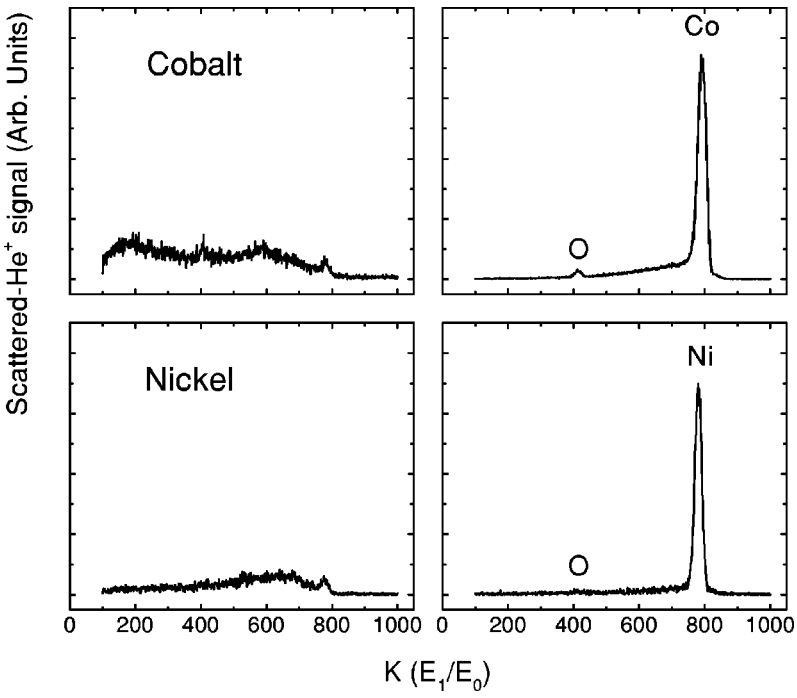

FIG. 2. Low-energy ion scattering spectra obtained after scattering of 2 keV He^+ on polycrystalline Co and Ni foils. The scattered ion signal is shown as function of the kinematic factor *K*, being the ratio of the kinetic energy of the He^+ ion after (E_1) and before (E_0) scattering. The spectra shown in the left column were taken prior to cleaning of the surface. The spectra in the right column are representative for essentially clean surfaces obtained after prolonged ion-beam sputter cleaning.

optically strong transitions. It should be noted that the use of a common intermediate state ensures a constant ionization volume experienced by atoms on all metastable states probed via this intermediate state. Saturation of the ionization step is hence not a requirement when applying this procedure but in order to increase drastically the efficiency of the ionization process, also the ionization transition is taken to be resonant

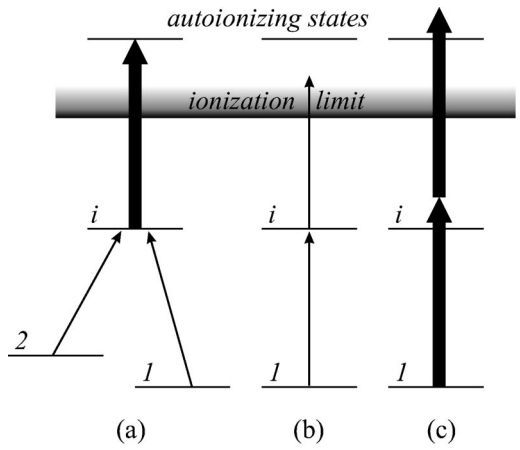

FIG. 3. (a) Schematic representation of the experimental procedure to determine the relative populations on states 1 and 2, by exciting the atoms in the two states to a common intermediate state *i*. Thin and thick arrows represent low, respectively, high-intensity laser light used to pump the transition. The sensitivity of the method is enhanced by tuning the ionization step to an autoionizing state above the first ionization limit. The signal obtained with the two-color scheme can contain a contribution from (b) the one-color two-step resonant scheme pumped by the excitation laser and starting from the selected intermediate state, and (c) the nonresonant scheme pumped by the ionization laser and addressing atoms on all populated metastable states.

by pumping the atoms in the excited state into an autoionizing state which is strongly coupled to the final continuum state. Unfortunately, for most elements with complicated electronic configurations, such as Co and Ni, these states are rarely tabulated. To devise double-resonant ionization schemes, the continuum structures of both elements were explored near their first ionization limits.[33,34] Since independently pumped laser systems are used, the correct sequence of the two steps in the applied ionization schemes can easily be checked by changing the time delay between the exciting and ionizing pulses. In all schemes used in this work, the photoion signal dropped to the sum of the one-color signals when the ionizing laser was fired before the exciting laser.

If in both steps photons are used with energies higher than half of the energy required to ionize a metastable atom, the ion signal as measured with a two-color scheme contains a contribution from the resonant one-color scheme using only the excitation laser [Fig. 3(b)] and a nonresonant contribution from direct two-photon ionization by the ionization laser [Fig. 3(c)]. Although the probability of the latter process is usually small, all atoms on all metastable states are addressed in this scheme. Care should thus be taken in selecting ionization schemes such that the amplification of the ionization efficiency is high, but at the same time nonresonant two-photon ionization is minimal. By measuring also the one-color ion signal, the two-color ion signal can be corrected for the nonresonant contribution. In principle, a nonresonant contribution from the excitation laser can also bias the two-color ion signal. Detuning the resonance showed that direct two-photon ionization by the low pulse energies generated with this laser is negligible.

When this procedure is generalized to address all metastable states, population distributions of overlapping subsets of metastable states have to be combined because only part of the metastable states can be coupled to a particular inter-

mediate state due to angular-momentum selection rules. Maximum ionization efficiency of state-selected atoms with parallel polarized laser light is achieved when atoms are transferred to a state with a higher statistical degeneracy.[28] If this could not be fulfilled, it was assumed that collisional mixing of the magnetic substates can be neglected and a correction factor α was introduced:

$$\alpha(g_1,g_i)=\begin{cases}1 & \text{if} \quad g_1 \leqslant g_i, \\ \dfrac{g_1}{g_i} & \text{if} \quad g_1 > g_i, \end{cases} \tag{1}$$

with g_1 and g_i the degeneracies of, respectively, the metastable state 1 and the intermediate state i. Since the population distributions are determined while sputtering the target with a long ion pulse (at least 3 μs duration), metastable atoms belonging to the same state-selected kinetic-energy distribution can be assumed to be homogeneously present in the ionization volume. If atoms in different states have different kinetic-energy distributions, our measurements do not directly reflect the relative sputter yields but rather the relative number densities of metastable atoms present in the ionization volume.[41]

Since each element has a unique set of atomic energy levels, the procedure described here to quantitatively measure the distribution of atoms over the metastable energy levels, in combination with time-of-flight mass spectrometry, is a highly element and state-selective detection technique applicable to both a pulsed and a continuous production of free atoms. Moreover, this technique can also be applied for state-selective photoionization of small molecules with sufficiently narrow spectral features.[38,39]

C. Flight-time distributions

From the flight time across a fixed distance l between the target and the laser-ionization volume the kinetic energy of a sputtered atom can be calculated. Quantum-state specific flight-time distributions are recorded by varying the delay between the moment of impact of a sufficiently short primary ion-pulse and the moment the ionizing laser pulse arrives in front of the target. The flight path l used in these experiments was typical 4 mm. Both the arrival of the ion pulse on the target and the laser pulse on a fast photodiode positioned at the experimental setup were recorded on an oscilloscope to determine the time difference between the moment of impact of the ion beam and the arrival of the laser pulse with an uncertainty of less than 50 ns.

Only when the ion and laser pulse would be infinitely short and the dimensions of the ion beam and the laser ionization volume infinitesimal, the experiment described above would allow us to determine the kinetic-energy flux distribution. However, since the ion and laser pulse have a finite duration and the ionization volume has finite dimensions, the measured ion signal will contain a contribution from the dynamic flux of the state-selected atoms through the laser-ionization volume and from the static density of these atoms inside the laser-ionization volume during the ionizing-laser pulses.[41] Because in our experiments relatively large laser beam diameters were used in combination with short laser pulse durations, the kinetic energy distributions are actually pure density distributions up to the highest kinetic energies ($\sim$50 eV) which can be determined accurately by this time-of-flight method. Within the accuracy of the method no differences between distributions measured with ion pulses from 100 up to 300 ns were observed. Simulations showed that ion pulses with durations longer than 500 ns will start to affect the flight-time distributions at low flight times (high kinetic energies).

When fast atoms leave the surface, the atomic transitions will be Doppler broadened. Since the ionization occurs parallel to the sample surface and the detection of sputtered atoms is restrained to a polar angle of max 10°, the full width at half maximum introduced by the Doppler effect is estimated to be less than 10 GHz for atoms with a kinetic energy of 30 eV and ionized using laser radiation of 300 nm. This is already less than the laser bandwidth and in many cases the transitions will be power broadened beyond this value, even at moderate laser fluences. To a good approximation we thus assume that atoms will have a velocity-independent excitation and ionization probability. The flight-time spectra are furthermore measured with the mass spectrometer in linear mode to exclude kinetic-energy dependent filtering effects that could be introduced by the reflectron.

IV. RESULTS

A. Saturation behavior

Prior to the actual probing of the population partitions of metastable Co and Ni atoms, we explored the continuum structure of these elements near the first ionization limit using two-color photoionization spectroscopy. In such experiments, the frequency of one laser is fixed to a resonant transition. By scanning the wavelength of the second laser, a large number of autoionizing states were observed. These states could only be partially identified but nevertheless allowed us to devise very efficient double-resonant ionization schemes.[33,34] In Fig. 4, partial energy level schemes for (a) Co I and (b) Ni I are presented, showing all metastable states and the selected intermediate multiplets together with the excitation steps used.

The saturation of all excitation and ionization steps was experimentally determined. Saturation of the excitation steps could be obtained for all transitions shown in Fig. 4 with the laser beam focused to a cross section of typically 3 mm^2 and with pulse energies of about 1 mJ. This is illustrated in Fig. 5(a) where the typical saturation behavior of excitation transitions for both elements is exemplified. These saturation curves were obtained by keeping the pulse energy of the ionizing laser at a constant value while varying the pulse energy of the exciting laser. Only well saturated transitions were used for the extraction of the relative population values. For the Co transitions pumped with UV light, the pulse energies used in the actual experiments to determine the population distributions were at least 3 to 4 times larger depending on the specific transition.

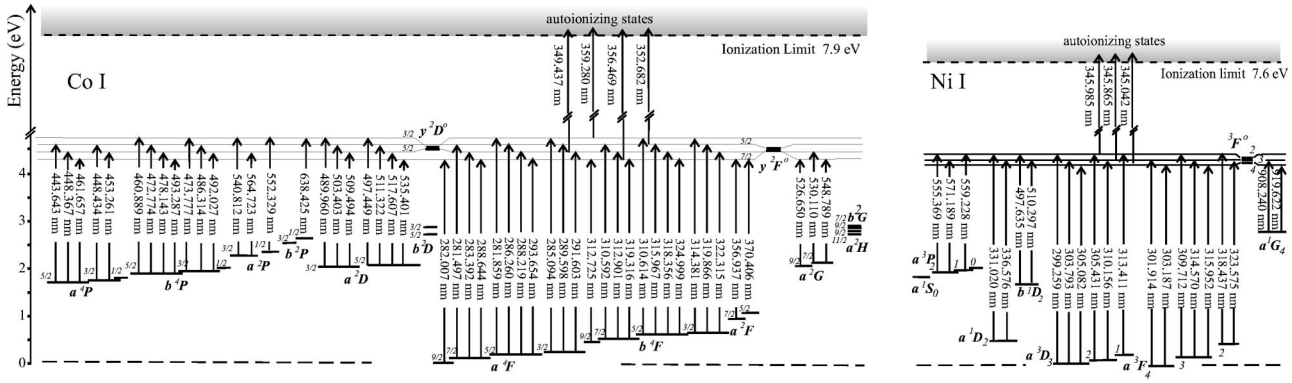

FIG. 4. Partial energy level scheme of Co I and Ni I. All metastable states and the employed intermediate multiplet are shown. The excitation and ionization steps that are used for the population partition measurements and their wavelengths are indicated.

The ionization steps could be saturated by tuning the ionizing laser to resonant transitions into autoionizing states. Also for these transitions saturation curves were determined, part of them are shown in Fig. 3(b). For a full overview of the saturation curves for all transitions, the reader is referred to Ref. 40.

B. Population distributions

The ionization schemes shown in Fig. 4 were applied to determine the population distributions of ground-state and metastable atoms. The validity and accuracy of the proposed experimental procedure was checked by determining the population distribution of a thermally evaporated ensemble. Therefore a pure Ni filament was introduced in the UHV chamber and resistively heated. The filament surface temperature [1470 (100) K] was measured with an optical pyrometer. In panel (c) of Fig. 6, the relative population, weighted with the ratio of the degeneracies of the ground state and the excited state, on low-lying metastable Ni states are presented as function of their excitation energy above the

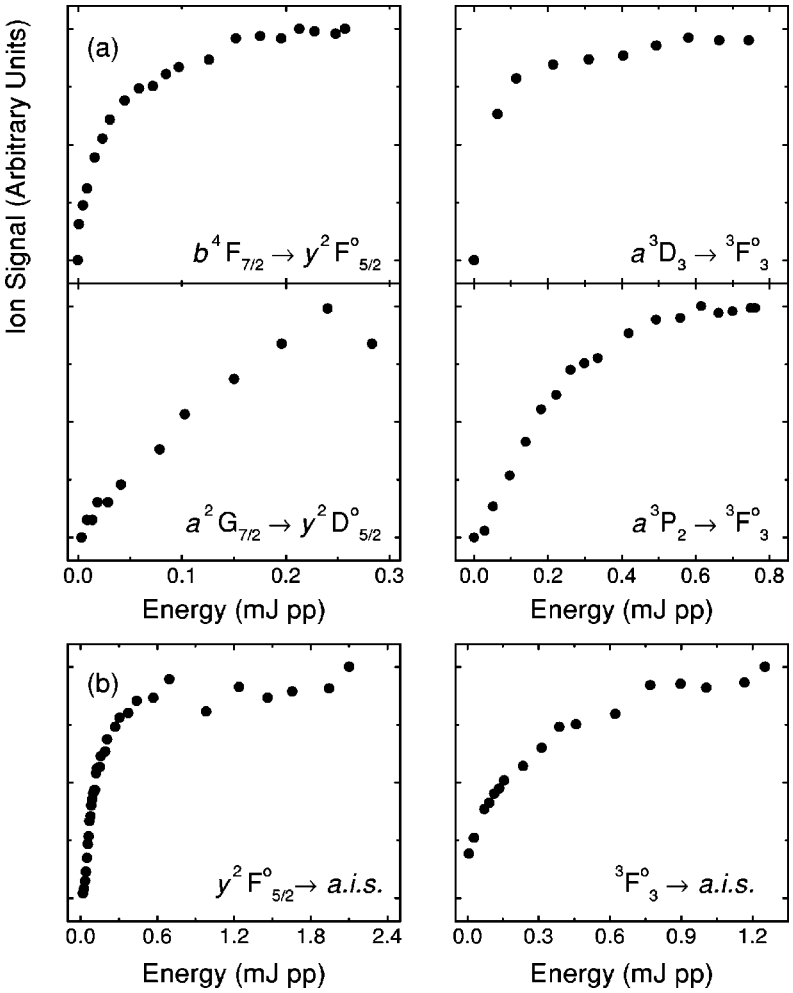

FIG. 5. Saturation behavior of (a) excitation transitions for Co (left column) and Ni (right column) as a function of the excitation laser energy with the pulse energy of the ionization laser kept constant and (b) ionization transitions into autoionizing states for Co (left column) and Ni (right column) as a function of the pulse energy of the ionizing laser system with the excitation laser saturating the excitation step.

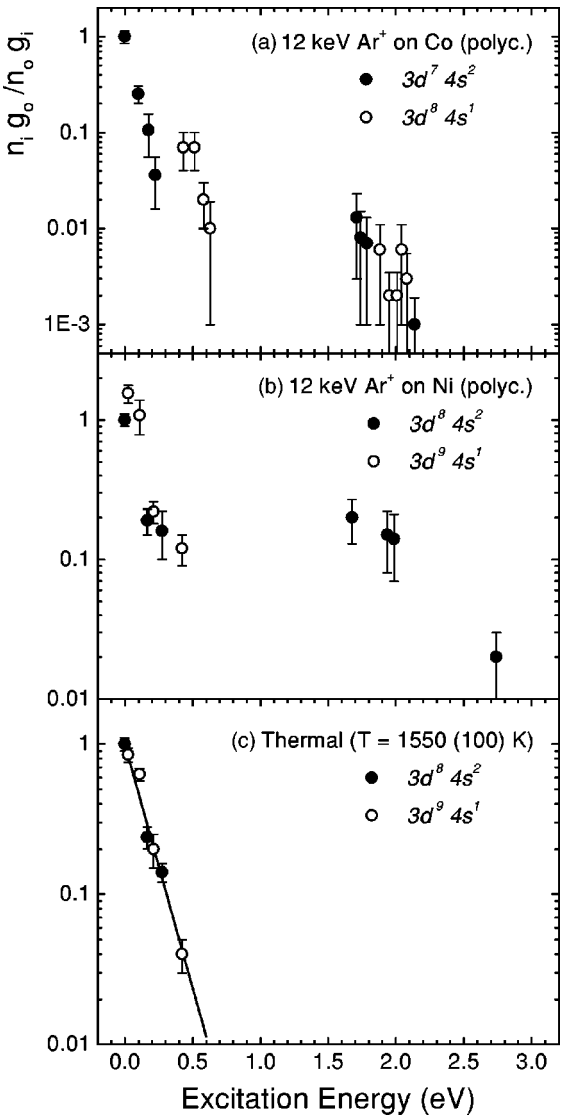

FIG. 6. The population distribution of Co (a) and Ni (b) metastable states for atoms produced by 12 keV Ar^+ sputtering of a clean polycrystalline foil and of Ni atoms produced by thermal evaporation of a pure wire (c). The populations (n_i) are given relative to the population on the ground state and are corrected for statistical weight (g_i). The open symbols refer to atomic states with electronic configurations with an partially filled outer *s* shell. The solid symbols refer to states with a completely filled outer *s* shell.

ground state in a semilogarithmic plot. Populations on higher excited states are below the relative detection limit of the apparatus (which is about 10^{-4}). The straight line in this figure is the best least-squares approximation of the Maxwell-Boltzmann thermal population distribution to the experimental data:

$$\frac{n_j}{n_0} = \frac{g_j}{g_0} \exp\left(\frac{E_j}{kT}\right), \tag{2}$$

where n_j/n_0 is the ratio of the number of atoms populating state j to the ground state population, g_j is the degeneracy and E_j the excitation energy of state j above the ground state (with excitation energy equal to zero), k is the Boltzmann constant and T the temperature of the ensemble of free atoms. The fit of Eq. (2) to the data yielded a temperature T of 1550 (100) K which is in perfect agreement with the pyrometric measurement. During the experiment, the pressure in the UHV chamber typically rose from 6×10^{-10} to 6×10^{-9} hPa due to evaporation and outgassing of the filament. This pressure rise is negligible and collisional quenching of the nickel atoms can be excluded.[42] This experiment is thus compelling evidence that the ensemble of evaporated atoms remains in thermal equilibrium with the surface of the filament.

The uncertainties on the values shown in Fig. 6 are mainly stemming from the standard deviations on the statistical averages obtained from different independent measurements, each involving one to three intermediate states. For some ionization schemes having high oscillator strenghts for the excitation step and strong coupling into the continuum states, a background due to resonant one-color two-step ionization has to be subtracted from the two-color signal. Because of slightly different ionization volumes, a state-dependent additional error of about 10% is added. The good agreement of the experimentally determined population partition with the Maxwell-Boltzmann distribution indicates that systematic errors, e.g., due to incomplete saturation of certain transitions, are absent within the estimated uncertainties.

The measured population distributions of Co and Ni ensembles after continuous ion-beam sputtering of clean polycrystalline Co and Ni foils with 15 keV Ar^+ ions are shown in Figs. 6(a) and 6(b) respectively. For both elements, states with different electronic configurations are denoted by different symbols. In Fig. 6(a), Co states with a completely filled outer shell, i.e., a $3d^74s^2$ configuration, are denoted by a solid symbol. In order of increasing excitation energy these are the a^4F_J multiplet to which the ground state belongs, the a^4P_J and a^2G_J states, with J referring to the total angular momentum of the state involved. Open symbols are used to denote the b^4F_J, b^4P_J, and the a^2D_J states with a partially filled outer shell, i.e., a $3d^84s^1$ configuration. The same convention is used in panel b of the figure to distinguish the Ni states with a $3d^84s^2$ outer shell configuration (solid symbols for the ground state multiplet a^3F_J, the b^1D_2, $a^3P_{1,2}$ and a^1G_4 states) from the states with a $3d^94s^1$ configuration (open symbols for the a^3D_J and a^1D_2 states).

The Co and Ni population distributions as obtained after sputtering show several a-thermal features. All metastable states with excitation energies up to 2.7 eV are highly populated. A distinction should be made between populations of the metastable states with low excitation energy, and populations of states with excitation energies above 1.5 eV. The population partition on low-lying states with the same electronic configuration of the outer shell follows roughly an exponential dependence as function of the excitation energy. The populations on states with a $3d^x4s^1$ (open symbols) are enhanced with comparison to the states with a $3d^{x-1}4s^2$ configuration (closed symbols), with $x=8$ for Co and $x=9$ for Ni. The anomalously high population on high-lying metastable states deviates from a simple extrapolation of the exponential dependence of the population on low-lying metastable states. Within the experimental accuracy, apparently

no clear differences in population of high-lying states with different electronic configurations of their outer shell are observed.

C. Flight-time distributions

Information on the kinetic energy of Co and Ni atoms emitted in the ground state as well as in most metastable states could be determined from experimentally obtained flight-time distributions. It is well known that the sputtered flux contains a substantial amount of clusters, with up to a few hundred atoms per cluster.[43–45] Upon formation, the majority of these nascent clusters spontaneously decomposes until only (meta)stable fragments remain. This unimolecular decomposition will already be terminated a few ns after the clusters are formed. This is well below the time window which is accessible in our experiments. However, the relative cluster yield is found to obey a power-law dependence on the cluster size. The yield of a cluster of size $n=10$ is typically already 4 orders of magnitude lower than the monomer yield.[45] Moreover, the dissociation threshold of the dimers, which form the second most abundant neutral species in the flux of sputtered particles, is of the order of 2 eV.[46] Extensive molecular dynamics simulations showed that the average internal energy of sputtered metal dimers is below 1 eV.[47] Only a small fraction of the sputtered dimers will thus have enough internal energy to decompose. Although it cannot be excluded that remains of dissociated clusters will finally contribute to the population of the metastable states, even the worst-case scenario cannot account for the total population on these states.

Laser probing of atoms by ionization in a strong laser field is also known to induce a velocity-independent photofragmentation of (meta)stable clusters and molecules present in the ionization volume. Although double-resonant ionization schemes were employed to keep the photon fluences at modest levels, the importance of photofragmentation cannot *a priori* be neglected. This contribution can be experimentally evaluated by determining the flight-time distributions of sputtered clusters. In Fig. 7, the flight-time distributions of ground-state and highly excited metastable sputtered Co and Ni atoms are compared with those of the sputtered dimers measured by nonresonant two-photon ionization. Both for Co and Ni, the dimer distributions are clearly shifted towards longer flight times compared to the monomer distributions, even for atoms occupying the high-lying metastable states. If photofragmentation of small clusters would be responsible for the population on these states, the flight-time distributions would be fully overlapping. The distinct difference between the distributions of the atoms and the dimers is clear evidence that photodissociation of sputtered small clusters largely can be neglected as the source of the population on these atomic states.

In Fig. 8, typical flight-time distributions are shown for Co and Ni atoms on different metastable states. For a full overview of the distributions, the reader is referred to Ref. 40 For both elements, it can be noted that the shape of the distribution for atoms on low-lying metastable states strongly depends on the electronic configuration. Co and Ni atoms with a partially filled outer shell configuration $3d^8 4s^1$ tend

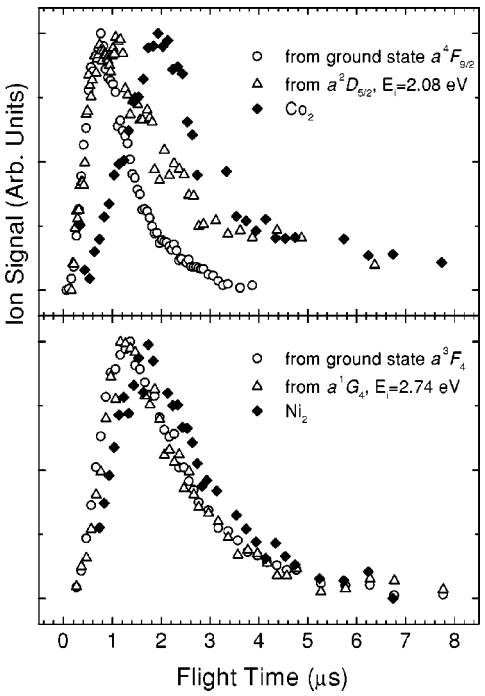

FIG. 7. Ion signal of sputtered photoionized ground and metastable Co (upper panel) and Ni (lower panel) atoms, and the respective dimers as function of the delay time between the ion pulse and the ionizing laser pulse.

to belong to distributions that rise and fall steeper while peaking at lower flight times compared to those of atoms with a completely filled outer shell. The flight-time distributions of atoms sputtered into high-lying metastable states all bear close resemblance with the distributions obtained for atoms in the ground state, irrespective of their electronic configurations.

V. DISCUSSION

A. Evaluation of the experimental procedure

The experiments presented here clearly demonstrate the versatility of laser ionization for sputter studies. Even ionization schemes depending on only one tunable laser system have been proven to be very valuable to enlarge the limited amount of reliable data on excited atoms formed during ion bombardment. In several cases the sensitivity has proven to be sufficiently high to compile accurately energy distributions, even with angular resolution.[9–17,22,24] However, the determination of population partitions is much less straightforward and previous attempts to determine the population of thermally produced atoms on metastable states using one-color two-step ionization were far less successful. In such schemes, atoms originally in different metastable states finally end up in different continuum states. We have shown previously that both Co and Ni continua exhibit a rich and complex structure of autoionizing states near the first ionization limit. This results in strongly wavelength dependent photoionization cross sections, leading to variations in pho-

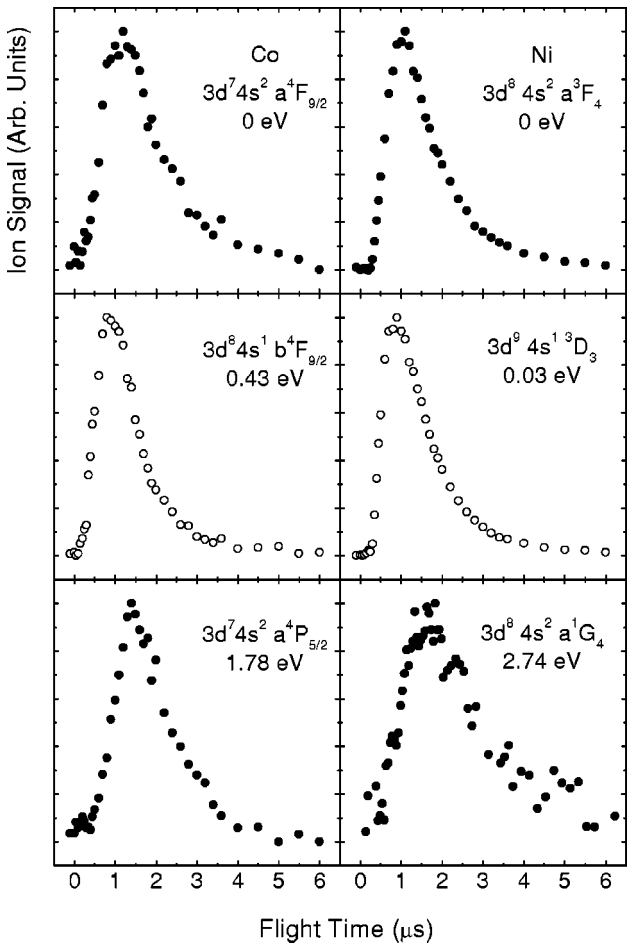

FIG. 8. Experimental flight-time distributions of sputtered (a) Co atoms and (b) Ni atoms in the ground and excited metastable states.

toion intensity of typically an order of magnitude when using different excitation routes originating from the same metastable state.

In principle, differences in photoionization efficiency cancel out when the ionization steps are driven into saturation. However, even if it is experimentally achievable to generate such high laser fluences, nonresonant ionization of atoms on other metastable states will strongly contribute to the measured photoion signal. By modeling the dynamics of stepwise photoionization by a density-matrix or rate-equation approach, the population on the initial state can be deduced from saturation measurements such as the ones shown in Fig. 5. This approach not only relies crucially on the theoretical model for the laser-energy dependence but even more on the cross sectional profile of the pulsed-laser beam, often approximated by a pure Gaussian. To quantify the surprisingly high population on a single, high-lying excited Ag state, this procedure was followed employing ionization schemes with strongly different ionization behavior for the ground and the metastable state.[19]

In another approach to encompass the variations in photoionization efficiency, the population distribution of sputtered Ni atoms was obtained by relating the photoion signals obtained in a sputter experiment to those from an experiment in which atoms were evaporated from a heated filament using the same ionization schemes.[16,25] Postulating that the atoms in the latter measurement originate from a Boltzmann-distributed ensemble, the overall detection efficiency can be eliminated from the comparison. As the thermal population on metastable states with excitation energies above 0.5 eV drops below the detection limit of this method, this procedure fails to quantify populations on highly-excited states, which are readily observed in sputtering experiments.

None of these drawbacks are present in the approach we outlined here as the relative populations directly follow from the measured photoion signals. The good agreement between the experimental population of the atoms released from a resistively heated filament with a Boltzmann distribution at a known temperature proved that the procedure is sufficiently reliable without the need of any *a priori* assumptions. The experimental procedure presented here should also become a valuable tool to help elucidate the physical processes involved in other atomization mechanisms such as laser sputtering. Up to now, only a very limited number of studies of laser sputtering by state-selective postionization techniques were reported. Especially in the sputtering regime where low laser intensities are used, some experiments indicate that nonthermal effects might play a prominent role.[5] The determination of the population partition in combination with flight-time distributions of state-selected atoms, as function of irradiating laser intensity or other parameters, might provide new and exciting results.

B. Interpretation of the sputtering data

1. Electronic processes during the emission of atoms

The experimental procedure presented here was successfully applied to obtain nearly complete sets of population partitions and flight-time distributions of sputtered Co and Ni atoms. The distinct athermal features observed in these experimental data sets urge to evaluate the electronic processes involved in the sputter process. Over the years different models including collisional-induced excitation and configuration-dependent deexcitation were proposed to account for the formation of excited atoms. None of these models can, however, fully account for the trends observed in the recent RIMS observations. For a more detailed discussion on the experimental data available and the evolution in the theoretical interpretation, the reader is referred to Ref. 48. The combined data can be interpreted as evidence for the dominant role of multichannel resonance electron transfer (RET) during sputtering.[49–51] Historically, RET has been the subject of many theoretical and experimental studies on *scattering* of atoms and molecules from metal surfaces. Several reviews on these topics have been published.[52,53] In *sputtering* studies, RET was invoked to explain the variation of sputtering yield of negative ions as a function of surface-adsorbate coverage.[54] Also, differences in population on highly excited atomic and ionic states were already interpreted by Veje to stem from preferential neutralization into states within an atomic energy window corresponding to the valence band of the solid.[55] Up to now, the complexity introduced by mul-

tiple parallel neutralization channels restrains us to go beyond a comparison of the data with the qualitative features of RET.

In the RET model the particles are considered to be sputtered initially as positive ions, strongly coupled to the metal. This coupling can be understood as the nonadiabatic tunneling of an electron between the conduction band of the unperturbed metal and the localized atomic energy states of the escaping particle up to the point where the interaction effectively stops and the final charge and/or excited state is settled. Of critical importance in this description is the position of the atomic energy level with respect to the Fermi level which separates occupied from unoccupied band states in the solid. Experimentally, all Co and Ni states lying within the energy window determined by the metal valence band are indeed substantially populated. Moreover, the exponential decrease of the population on the states within each low-lying multiplet indicates that the energy difference between the Fermi level and the atomic level i (given by $I-\Phi-E_i$, with I the first ionization potential of the element, Φ the work function of the metal and E_i the excitation energy of the atomic state above the ground state of the neutral atom) governs the competition between the different neutralization channels within one multiplet. The probability that an electron neutralizes an escaping ion in a particular electronic configuration is determined by the magnitude of the matrix element that expresses the coupling between the initial state in the metal and the final atomic state. A good spatial overlap between the wave functions of the states involved ensures large overlap integrals and thus favors population of the final state. Both for Co and Ni, the valence band states have a dominant $3d^x4s^1$ character which explains an enhanced population on the atomic states with a $3d^x4s^1$ configuration.[56,57] Additional evidence for a state-dependent neutralization probability comes from the measured flight-time distributions. The neutralization efficiency by electron tunneling into states that lie sufficiently low in the energy window, is expected to be smaller the faster the atom recedes from the surface.[52] The higher the particle's velocity, the shorter the interaction time, and the less probable that an electron will be transferred into atomic states that are weakly coupled with the bulk. This will lead to the systematic shift towards short flight times (i.e., short interaction times) observed in the flight-time distributions of Co and Ni atoms sputtered in low-lying $3d^x4s^1$ states. For long interaction times, the influence of , e.g., the relative level positions with respect to the Fermi level could become the dominant factor, reducing the influence of the electronic configuration.

Also, when the energy difference between the atomic energy level and the Fermi energy becomes smaller, i.e., when the atomic state lies close to the top of the energy window, detailed features such as the level shift and broadening or the electron density near the surface will start to influence more dominantly the electron-transfer probability. Other excitation and deexcitation events thus could become competitive with or even blur the simple electron-transfer picture proposed here.

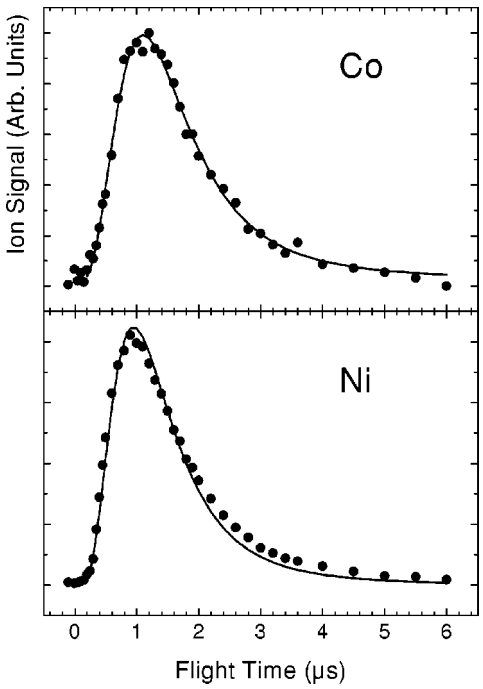

FIG. 9. Weighted sum of state-specific flight-time distributions (dots) of sputtered Co (upper panel) and Ni (lower panel) columns, compared to the Thompson distribution (solid lines).

2. Surface binding energy

From collision-cascade theory, the kinetic energy flux distribution of sputtered particles at the low-energy part of the collision cascade is given by the Thompson distribution[6,7]

$$F_T(E) \propto \frac{E}{(E+U)^3} \tag{3}$$

with E the kinetic energy of the sputtered particle and U the surface binding energy. Using the suitable Jacobian and the known length of the flight path l and the mass m of the sputtered particle, distribution Eq. (3) can be rewritten as a flight-time density distribution

$$f_T(t) \propto \frac{(l/t)^4}{\left[\frac{m}{2}(l/t)^2+U\right]^3}. \tag{4}$$

Although strictly speaking only applicable for particles that are sputtered from an amorphous target with an isotropic velocity distribution through a planar surface barrier, experimental distributions obtained from pure polycrystalline metals show quite good agreement with the Thompson distribution. Velocity-dependent resonant electron transfer introduces a configurational-dependent shape of the flight-time distributions $f_i(t)$ of atoms sputtered into a particular fine structure state i. However, if we assume the contribution of secondary ions in the total number of sputtered particles to be small, the sum of the state-specific flight-time distributions weighted with their respective populations n_i should to a good approximation correspond to the Thompson distribution[50]

$$f_{\mathrm{tot}}(t) \propto \sum_i n_i f_i(t) \propto f_T(t). \quad (5)$$

Such weighted Co and Ni distributions are indeed found to be in good accordance with the predictions of the linear cascade theory, as can be seen in Fig. 9. The binding energy obtained from the least-squares fit of Eq. (5) to the experimental distribution, was found to be 2.7 (5) eV for Co and 3.8 (5) eV for Ni. The value obtained for Ni is in accordance with other sputtering experiments using one-color two-step laser photoionization.[16,25] For many metals, the surface binding energy is experimentally found to be close to the sublimation energy. For Co and Ni this value is equal to 4.4 eV. The deviation of the Ni binding energy from this value was previously attributed to the formation of a nickel carbide surface layer during the experiment.[25] However, as mentioned before from the separate LEIS and *in situ* SIMS measurements we can conclude that, after carefully cleaning the sample prior and during the experiments by prolonged ion-beam bombardment, no carbon atoms could be detected within the instrumental detection limits of these techniques.

VI. CONCLUSIONS

In summary, we reported the use of double-resonant laser ionization spectroscopy to systematically study population partitions and kinetic energy distributions of atoms in the ground and metastable electronic states. The experimental procedure was illustrated with a study the population partition of metastable Ni and Co atoms during different atomization processes. The accuracy and reliability of the proposed experimental procedure was proved by the correct determination of the temperature of a thermally evaporated atomic Ni ensemble by probing the population partition of the atoms in the ground and metastable states. Population partitions and time-of-flight distributions of Co and Ni atoms sputtered from clean polycrystalline material with 15 keV Ar^+ ions, were measured. Atoms were found to be ejected preferentially into states with electronic configurations that resemble closely the configuration of the band structure of the solid. The populations on very high-lying metastable states could be systematically measured and were found to be anomalously high. The combined interpretation of these distributions allowed to account for resonant transfer of electrons from the metal to the sputtered particle as being a dominant population mechanism during keV ion-beam sputtering of metals.

ACKNOWLEDGMENTS

The authors wish to thank H. Tollet, Afdeling Fysische Scheikunde of the Departement Chemische Ingenieurstechnieken, K. U. Leuven, for performing the LEIS measurements. We gratefully acknowledge stimulating discussions with N. Winograd, B.J. Garrison, A. Wucher, and Z. Postawa. This work was financially supported by the Fund for Scientific Research—Flanders (F.W.O.) and by Flemish Concerted Action (G.O.A.) and Inter-University Attraction Pole (I.U.A.P.) Research Programs.

[1] *Sputtering by Particle Bombardment I*, edited by R. Behrisch, Vol. 47 of Topics in Applied Physics (Springer, Berlin, 1981).
[2] *Sputtering by Particle Bombardment II*, edited by R. Behrisch, Vol. 52 of Topics in Applied Physics (Springer, Berlin, 1983)
[3] *Sputtering by Particle Bombardment III*, edited by R. Behrisch and K. Wittmaack, Vol. 64 Topics *Applied Physics* (Springer, Berlin, 1991).
[4] P. Sigmund, Mat. Fys. Medd. Dan. Vidensk Selsk. **43**, 1 (1993).
[5] R.F. Haglund and R. Kelly, Mat. Fys. Medd. Dan. Vidensk. Selsk. **43**, 527 (1993).
[6] M. Thompson, Philos. Mag. **18**, 377 (1968).
[7] P. Sigmund, Phys. Rev. **184**, 383 (1969).
[8] M.L. Yu in *Sputtering by Particle Bombardment III*, Vol. 64 of *Topics in Applied Physics*, edited by R. Behrisch, and K. Wittmaack, (Springer, Berlin, 1991) 91.
[9] B.I. Craig, J.P. Baxter, J. Singh, G.A. Schick, P.H. Kobrin, B.J. Garrison, and N. Winograd, Phys. Rev. Lett. **57**, 1351 (1986).
[10] R. Maboudian, Z. Postawa, M. El-Maazawi, B.J. Garrison, and N. Winograd, Phys. Rev. B **42**, 7311 (1990).
[11] M. El-Maazawi, R. Maboudian, Z. Postawa, and N. Winograd, Phys. Rev. B **43**, 12 078 (1991).
[12] D.N. Bernardo, M. El-Maazawi, R. Maboudian, Z. Postawa, N. Winograd, and B.J. Garrison, J. Chem. Phys. **97**, 3846 (1992).
[13] N. Winograd, M. El-Maazawi, R. Maboudian, Z. Postawa, D.N. Bernardo, and B.J. Garrison, J. Chem. Phys. **96**, 6314 (1992); **100**, 8557 (1994).
[14] C. He, Z. Postawa, M. El-Maazawi, S. Rosencrance, B.J. Garrison, and N. Winograd, J. Chem. Phys. **101**, 6226 (1994).
[15] S.W. Rosencrance, J.S. Burnham, D.E. Sanders, C. He, B.J. Garrison, N. Winograd, and A.E. DePristo, Phys. Rev. B **52**, 6006 (1995).
[16] C. He, Z. Postawa, S.W. Rosencrance, R. Chatterjee, B.J. Garrison, and N. Winograd, Phys. Rev. Lett. **75**, 3950 (1995).
[17] C. He, S.W. Rosencrance, Z. Postawa, C. Xu, R. Chatterjee, D.E. Riederer, B.J. Garrison, and N. Winograd, Nucl. Instrum. Methods Phys. Res. B **100**, 209 (1995).
[18] G. Nicolussi, W. Husinsky, D. Gruber, and G. Betz, Phys. Rev. B **51**, 8779 (1995).
[19] W. Berthold and A. Wucher, Phys. Rev. Lett. **76**, 2181 (1996).
[20] W. Berthold and A. Wucher, Nucl. Instrum. Methods Phys. Res. B **115**, 411 (1996).
[21] E. Vandeweert, V. Philipsen, W. Bouwen, P. Thoen, H. Weidele, R.E. Silverans, and P. Lievens, Phys. Rev. Lett. **78**, 138 (1997).
[22] W. Berthold, and A. Wucher, Phys. Rev. B **56**, 4251 (1997).
[23] P. Lievens, V. Philipsen, E. Vandeweert, and R.E. Silverans, Nucl. Instrum. Methods Phys. Res. B **135**, 471 (1998).
[24] B.V. King, C. Zimmerman, D.E. Riederer, S.W. Rosencrance, B.J. Garrison, and N. Winograd, Rapid Commun. Mass Spectrom. **12**, 1236 (1998).
[25] A. Cortona, W. Husinsky, and G. Betz, Phys. Rev. B **59**, 15 495 (1999).

[26] A. Goehlich, A. Goehlich, and H.F. Döbele, Nucl. Instrum. Methods Phys. Res. B **164-165**, 827 (2000).
[27] D. Ishikawa, R. Ishigami, S.D. Dhole, and K. Morita, Nucl. Instrum. Methods Phys. Res. B **164-165**, 840 (2000).
[28] M.G. Payne, Lu Deng, and N. Thonnard, Rev. Sci. Instrum. **65**, 2433 (1994).
[29] E.B. Salomon, Spectrochim. Acta B **45**, 37 (1990).
[30] E.B. Salomon, Spectrochim. Acta B **46**, 319 (1991).
[31] E.B. Salomon, Spectrochim. Acta B **47**, 517 (1992).
[32] E.B. Salomon, Spectrochim. Acta B **48**, 1139 (1993).
[33] P. Lievens, E. Vandeweert, P. Thoen, and R.E. Silverans, Phys. Rev. A **54**, 2253 (1996).
[34] E. Vandeweert, P. Lievens, V. Philipsen, and R.E. Silverans, Spectrochim. Acta B **54**, 1219 (1999).
[35] A. Benninghoven, K.H. Müller, M. Schemmer, and P. Beckmann, Appl. Phys. **16**, 367 (1978).
[36] E. Taglauer, Appl. Phys. **51**, 238 (1990).
[37] Y. Yamamura and H. Tawara, At. Data Nucl. Data Tables **62**, 149 (1996).
[38] C.A. Meserole, E. Vandeweert, R. Chatterjee, B.R. Chakraborty, B.J. Garrison, N. Winograd, and Z. Postawa, in *Resonance Ionization Spectroscopy*, edited by John C. Vickerman *et al.*, AIP Conf. Proc. **454** (AIP, Woodbury, NY, 1998), p. 210.
[39] E. Vandeweert, C.A. Meserole, A. Sostarecz, Y. Dou, N. Winograd, and Z. Postawa, Nucl. Instrum. Methods Phys. Res. B **164-165**, 820 (2000).
[40] See AIP Document No. E-PAPS: E-PRBMDO-64-051139 for a full overview of both the saturation curves and the flight-time distributions. This document may be retrieved via the EPAPS homepage (http://ww.aip.org/pubservs/epaps.html) or from ftp.aip.org in the directory /epaps/. See the EPAPS homepage for more information.
[41] A. Wucher, M. Wahl, and H. Oechsner, Nucl. Instrum. Methods Phys. Res. B **82**, 337 (1993).
[42] *Atomic and Molecular Beam Methods Volume I*, edited by G. Scoles (Oxford University Press, New York, 1988).
[43] W. O. Hofer in *Sputtering by Particle Bombardment III*, edited by R. Behrisch, and K. Wittmaack, Topics in Applied Physics No. 64 (Springer, Berlin, 1991), p. 15.
[44] H.M. Urbassek, Mat. Fys. Medd. Dan. Vidensk. Selsk. **43**, 97 (1993).
[45] C. Staudt, R. Heinrich, and A. Wucher, Nucl. Instrum. Methods Phys. Res. B **164-165**, 677 (2000).
[46] J.C. Pinegar, J.D. Langenberg, C.A. Arrington, E.M. Spain, and M.D. Morse, J. Chem. Phys. **102**, 666 (1995).
[47] A. Wucher, N. Kh. Dzhemilev, I.V. Veryovkin, and S.V. Verkhoturov, Nucl. Instrum. Methods Phys. Res. B **149**, 285 (1999).
[48] B.J. Garrison, N. Winograd, R. Chatterjee, Z. Postawa, A. Wucher, E. Vandeweert, P. Lievens, V. Philipsen, and R.E. Silverans, Rapid Commun. Mass Spectrom. **12**, 1266 (1998).
[49] R. E. Silverans and P. Lievens, in *Resonance Ionization in Spectroscopy* (Ref. 38), p. 197.
[50] V. Philipsen, J. Bastiaansen, E. Vandeweert, P. Lievens, and R.E. Silverans, in *Resonance Ionization Spectroscopy* (Ref. 38), p. 353.
[51] E. Vandeweert, J. Bastiaansen, Vicky Philipsen, P. Lievens, and R.E. Silverans, Nucl. Instrum. Methods Phys. Res. B **164-165**, 795 (2000); V. Philipsen, J. Bastiaansen, P. Lievens, E. Vandeweert, and R.E. Silverans, Vacuum **56**, 269 (2000).
[52] J. Los and J.J.C. Geerlings, Phys. Rep. **190**, 133 (1990).
[53] J.P. Gauyacq and A.G. Borisov, J. Phys.: Condens. Matter **10**, 6585 (1998).
[54] M.L. Yu, D. Grischkowsky, and A.C. Balant, Phys. Rev. Lett. **48**, 427 (1982).
[55] E. Veje, Phys. Rev. B **28**, 88 (1983); P. Larsen and E. Veje, *ibid.* **28**, 5011 (1983); E. Veje, *ibid.* **28**, 5029 (1983).
[56] J.W.D. Conolly, Phys. Rev. **159**, 415 (1967).
[57] L.F. Mattheiss, Phys. Rev. **134**, A970 (1964).